

# Accurate curve fits of IAPWS data for high-pressure, high-temperature single-phase liquid water based on the stiffened gas equation of state

J. W. Peterson<sup>\*1</sup>

<sup>1</sup>Idaho National Laboratory

November 5, 2013

## Abstract

We present a series of optimal (in the sense of least-squares) curve fits for the stiffened gas equation of state for single-phase liquid water. At high pressures and (subcritical) temperatures, the parameters produced by these curve fits are found to have very small relative errors: less than 1% in the pressure model, and less than 2% in the temperature model. At low pressures and temperatures, especially near the liquid-vapor transition line, the error in the curve fits increases rapidly. The smallest pressure value for which curve fits are reported in the present work is 25 MPa, high enough to ensure that the fluid remains a single-phase liquid up to the maximum subcritical temperature of approximately 647K.

## 1 Introduction

The stiffened gas equation of state is frequently used in the simulation of compressible liquids, in particular water [1], but can also be used for simulating compressible gases including water vapor and air. It is attractive

---

<sup>\*</sup>jw.peterson@inl.gov

primarily due to the fact that it is a generalization of the ideal gas equation of state, and because of its simplicity: only four independent constants ( $\gamma$ ,  $q$ ,  $p_\infty$ , and  $c_v$ ) are required to define the pressure and temperature models, which are given by

$$p = (\gamma - 1)\rho(e - q) - \gamma p_\infty \quad (1)$$

$$T = \frac{1}{c_v} \left( e - q - \frac{p_\infty}{\rho} \right) \quad (2)$$

where  $p$  is pressure,  $T$  is temperature,  $\rho$  is density, and  $e$  is the internal energy of the fluid. We note that a fifth constant, denoted  $q'$ , is required to model the Gibbs free enthalpy, however this quantity is not needed for performing typical thermohydraulic calculations. The parameter  $c_v$  used in (2) should not be confused with its typical meaning, i.e. the fluid's specific heat at constant volume. Rather, we shall treat it as a free parameter in the curve fitting process to be described subsequently.

For reference, the squared sound speed  $c^2$ , generalized adiabatic coefficient  $\gamma^*$ , Grüneisen coefficient  $\Gamma$ , and fundamental derivative  $\mathcal{G}$  [2] for the stiffened gas equation of state are given by

$$c^2 = \frac{p + p_\infty}{\rho} \quad (3)$$

$$\gamma^* = \gamma \left( \frac{p + p_\infty}{p} \right) \quad (4)$$

$$\Gamma = \gamma - 1 \quad (5)$$

$$\mathcal{G} = \frac{1}{2} (\gamma + 1) \quad (6)$$

The quantities (3)–(6) coincide with their well-known values for the ideal gas equation of state when  $p_\infty = 0$ , and imply an *a priori* restriction on any curve fits computed for the model: they must have  $\gamma > 1$  in order for the usual assumptions on  $\Gamma$ , i.e.  $\Gamma > 0$ , to hold.

Although the four parameters in (1) and (2) are treated as constants in practice, in reality they are weak functions of both pressure and temperature for an actual fluid — especially far from phase transition boundaries. Although various numerical values for the constants have been proposed previously in the literature [3], it appears that no systematic curve fits (with well-quantified relative error bounds) have thus far been published for the stiffened gas equation of state for water.

A schematic of the basic phase diagram structure of water is given in Fig. 1. The curve fits in this paper are valid only in the “compressible liquid” region of the diagram, i.e. for pressures above the critical pressure (which for water is approximately 22.064 MPa) and below the critical temperature of approximately 647K. For lower pressures, especially near the liquid-vapor transition line, it was found that curve fits based on the stiffened gas equation of state had unacceptably high relative error levels. A key observation is the following: the relative simplicity of the stiffened gas equation of state leads to a tradeoff in its overall applicability. If accurate state values near the phase transition line are required (as is often the case in multi-phase flows) a more sophisticated model, such as the modified Tait equation of state [4, 5] should be employed.

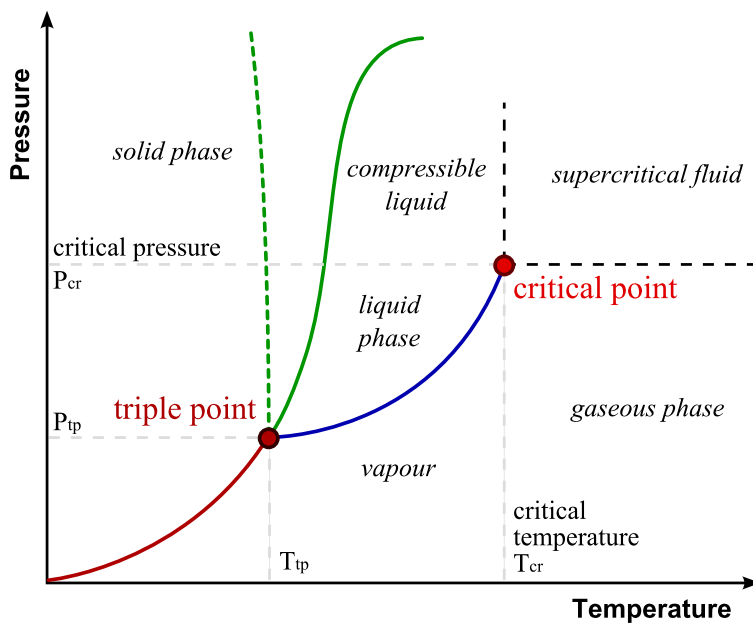


Figure 1: Schematic phase diagram of water [6].

The remainder of this paper is organized in the following way: in §2, we describe the functional form of the curve fits, and the normalized linear least-squares fitting procedure used in computing them. Then, in §3, the resulting fits are provided in the form of line plots and tabulated values, along with some discussion of how they can be utilized effectively. Finally,

in §4, we discuss the limitations of the stiffened gas equation of state near phase transition boundaries, and give some suggestions for future work.

## 2 Methodology

In this section, we describe some general strategies for fitting multiple models simultaneously, the specific least-squares optimization problems solved in the present work, and the data gathering and relative error measures used in creating the fits.

### 2.1 Fitting Strategy

Selecting a curve fitting strategy for (1) and (2) does not appear to be a straightforward process: because there are two models that involve a partially-overlapping set of fit parameters, it is reasonable to ask whether one can find a *single* set of fit parameters which is *simultaneously* optimal (in some sense) for both models. This problem may be characterized in the framework of “multi-objective” optimization [7].

Multi-objective optimization algorithms are useful in situations where improvements in one objective function lead to degradation in one or more of the other objective functions. The solution to a given multi-objective optimization problem is the set of so-called “Pareto optimal” or “Pareto efficient” [8] points in optimization space: points for which no one objective function can be improved without making one or more of the other objective functions worse.

These algorithms typically require the definition of an aggregate objective function, which is essentially a subjective choice on the part of the user. Furthermore, only a single set of parameters can be selected from among the (possibly large) set of all Pareto optimal parameter sets, and this choice is, again, subjective. Multi-objective optimization problems also frequently employ evolutionary (genetic) algorithms which are considerably more sophisticated than linear least-squares optimization.

In the present work, we instead employ the following “decoupled” fitting strategy:

1. Compute the set  $\{\gamma, q, p_\infty\}$  for which the pressure fit (1) is least-squares optimal.

2. Using the parameters computed in part 1, compute  $c_v$  for which the temperature fit (2) is least-squares optimal.

The philosophy behind this approach is fairly simple: solution of the Euler equations (a frequent use-case) requires only a pressure model. The temperature model is required whenever a thermal conduction term is present in the energy conservation equation; for example when solving the full Navier-Stokes equations, or when a wall-heating term is used to model heat transfer along the length of a pipe in 1D. Therefore, we make the arbitrary choice to let the pressure fit be least-squares optimal, and the temperature fit be “as good as it can be” given an optimal pressure fit. Of course, there is no reason to expect the temperature curve fits obtained in such a manner to have an acceptable amount of relative error over the entire fit range, nevertheless, in §3 we will demonstrate that this strategy is indeed capable of producing reasonable results.

## 2.2 Normalized Least-Squares Curve Fits

We can write (1) in terms of the internal energy,  $e$ , and the specific volume  $v \equiv \frac{1}{\rho}$  as

$$e = Apv + Bv + C \tag{7}$$

where

$$A = \frac{1}{\gamma - 1} \tag{8}$$

$$B = \frac{\gamma p_\infty}{\gamma - 1} \tag{9}$$

$$C = q \tag{10}$$

Clearly, (7) demonstrates that the internal energy is a “degenerate bilinear” function of  $p$  and  $v$  (with no term linear in  $p$ ), and is linear in the fit parameters  $A$ ,  $B$ , and  $C$ . Thus it is theoretically possible to compute  $A$ ,  $B$ , and  $C$  values which produce a least-squares optimal fit of the “data”  $e_i$  at specific points  $(p_i, v_i)$ , for  $i = 1, \dots, N$ . The stiffened gas parameters can then be

obtained from  $A$ ,  $B$ , and  $C$  as

$$\gamma = \frac{1}{A} + 1 \quad (11)$$

$$p_\infty = \frac{(\gamma - 1)B}{\gamma} \quad (12)$$

$$q = C \quad (13)$$

Unfortunately, attempting to compute fits of (7) using non-normalized data leads to extremely ill-conditioned least-squares matrices, and therefore unacceptable amounts of round-off error. We therefore instead consider the least-squares problem of finding  $A^*$ ,  $B^*$ , and  $C^*$  such that

$$e^* = A^*p^*v^* + B^*v^* + C^* \quad (14)$$

is least-squares optimal, where

$$e^* \equiv \frac{e - \mu_e}{\sigma_e} \quad (15)$$

$$p^* \equiv \frac{p - \mu_p}{\sigma_p} \quad (16)$$

$$v^* \equiv \frac{v}{\mu_v} \quad (17)$$

where  $\mu_x$  and  $\sigma_x$  are the mean and standard deviation of the variable  $x$ , respectively. Note that we arbitrarily select a linear (rather than affine) scaling for the specific volume variable, since upon expanding (14) we obtain

$$e = \underbrace{\frac{\sigma_e A^*}{\sigma_p \mu_v}}_A p v + \underbrace{\frac{\sigma_e}{\mu_v} \left( B^* - \frac{A^* \mu_p}{\sigma_p} \right)}_B v + \underbrace{(\mu_e + \sigma_e C^*)}_C \quad (18)$$

i.e. a form identical to the original model (7), with shifted and scaled coefficients. That is, there is a direct correspondence between the scaled fit parameters  $A^*$ ,  $B^*$ , and  $C^*$ , and the original fit parameters  $A$ ,  $B$ , and  $C$ , which is shown in (18). Using an affine transformation for  $v^*$  does not lead to such an isomorphism. The actual scalings used are, of course, arbitrary: the same fit will be produced regardless of the scaling employed. We merely require that the scaling improve the conditioning of the least-squares problem enough to produce sufficiently accurate solutions.

The basic procedure in determining the pressure fit is thus as follows:

1. Compute  $A^*$ ,  $B^*$ , and  $C^*$  in the normalized variables using (14)
2. Compute  $A$ ,  $B$ , and  $C$  using the relationships in (18)
3. Compute  $\gamma$ ,  $q$ , and  $p_\infty$  using (11)–(13)

Once  $\gamma$ ,  $q$ , and  $p_\infty$  are known, the model for  $T$  can be written as a function of  $e$  and  $v$  as

$$T = D(e - q - p_\infty v) \quad (19)$$

where  $D \equiv \frac{1}{c_v}$ . A single-parameter least-squares fit can then be used to determine  $D$  (and thus  $c_v$ ). In contrast to the pressure fit, the conditioning of this least-squares problem is not a concern since it reduces to a single scalar equation. Therefore we do not pursue a normalized fit for (19) as was done in the pressure model case, although an isomorphism results under the change of variables  $T^* = \frac{T}{\mu_T}$ . The lack of “degrees of freedom” available for the temperature fit is a direct consequence of the decoupled approach taken in obtaining the fits. We observe that the temperature fit will only be accurate if  $T \propto e - q - p_\infty v$ , a fact that is certainly not guaranteed by the parameters  $q$  and  $p_\infty$  which were optimal for the pressure fit.

### 2.3 Fit Data and Relative Error Measures

The data used in the present work come from the International Association for the Properties of Water and Steam (IAPWS) standard [9, 10], which are freely available online from NIST’s website<sup>1</sup>. Isobaric data for  $25 < p < 300$  MPa (in 5 MPa increments) and  $300 < T < 625$  (in 1 Kelvin increments) were obtained from the site and used in making the fits. Obviously, the amount and distribution of the data has a direct effect on the accuracy of the resulting fits. The pressure fit parameters were found (via trial and error) not to depend greatly on the granularity of the pressure data when the increments were less than about 5 MPa. Furthermore, away from the phase transition lines, the internal energy is a nearly linear function of both pressure and temperature, suggesting that the models (1) and (2) are indeed appropriate.

---

<sup>1</sup><http://webbook.nist.gov/chemistry/fluid>

We use the following relative error measure to judge the suitability of the curve fits produced by the methods described in this section:

$$\varepsilon_p \equiv \frac{\|\mathbf{p}_m - \mathbf{p}\|}{\|\mathbf{p}\|} \quad (20)$$

where  $\mathbf{p}_m$  is a vector of pressure model values as determined by the fit (7),  $\mathbf{p}$  is the vector of (known) pressure data values at corresponding points, and  $\|\cdot\|$  is the discrete  $\ell_2$ -norm. An analogous form is used to measure the error in the temperature fits. We (arbitrarily) consider fits with less than about 2% relative error to be suitable for numerical calculations, but of course this threshold depends on the application in question. The suitability of fits is, in general, also subject to other criteria: for example it is desirable that the fit models not produce negative (non-physical) values of pressure and temperature for any data points within the range of applicability. The fit parameters presented in this paper all satisfy this criterion.

### 3 Results and Discussion

The results of the least-squares curve fitting process described in §2 are presented graphically in Figures 2–5. The fits themselves were computed over 25 MPa pressure ranges (from data in 5 MPa increments) and 25 Kelvin temperature ranges (from data in 1 K increments). Each of the fit parameters is plotted vs. temperature for the various pressure ranges considered. The figures confirm that each of the optimal fit parameters is indeed a function of both pressure and temperature over the region of phase space under consideration, rather than a single constant as posited by the stiffened gas equation of state.

The slopes of the various fit parameter curves have varying levels of dependence on the pressure level. The slope of the  $p_\infty$  curves is almost independent of the pressure level; for this parameter, increased pressure levels lead to a constant offset in  $p_\infty$  over the entire range of temperatures tested. For the  $q$  and  $c_v$  parameters, the pressure effect is a bit stronger, and increasing pressure tends to “flatten” the curves:  $q$  (resp.  $c_v$ ) values at low temperatures decrease with increasing pressure while  $q$  (resp.  $c_v$ ) values at high temperatures tend to increase with increasing pressure. At high temperatures, the  $\gamma$  parameter behaves somewhat differently depending on the pressure. For higher pressures, the  $\gamma$  curves “bend downward” much less than at lower



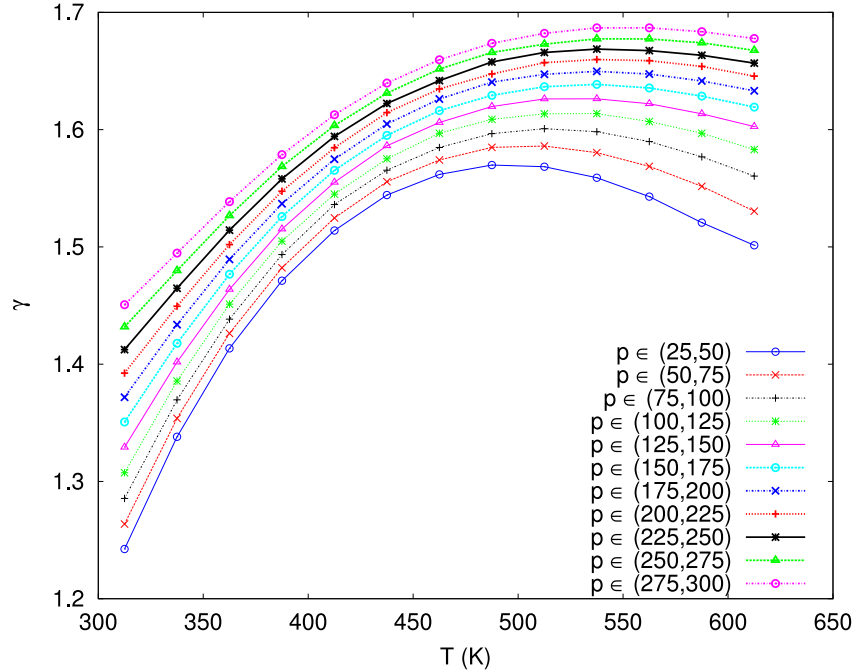


Figure 2: Plots of  $\gamma$  (dimensionless) vs. temperature for different pressure ranges, all pressure ranges are in MPa.

pressures. In general, the fits all improve with increasing pressure, since the fit parameters are more nearly constant at high pressures.

The total variation in  $\gamma$  due to temperature is slightly more than the amount of variation in  $\gamma$  due to pressure. For example, in the temperature range  $400 < T < 425$ ,  $\gamma$  varies between approximately 1.54 and 1.64 ( $\approx 6\%$ ) over the entire range of pressure values, but for a given pressure range, say  $275 < p < 300$  MPa,  $\gamma$  varies between 1.45 and 1.68 ( $\approx 13.7\%$ ). The total variations in  $c_v$  and  $q$  for the lowest pressure range ( $25 < p < 50$  MPa, where the highest variation occurs) over the entire temperature range are considerable: 93% and 98%, respectively. The  $q$  and  $c_v$  parameters both vary most rapidly at low temperatures, and therefore we expect the curve fit errors to be overall higher at lower temperatures. Numerical values for the data plotted in Figures 2–5 are given in Tables 1–4.

Figures 6 and 7 give plots of relative temperature and pressure errors (as defined by (20)) as functions of pressure for the different temperature ranges considered. While the plots in Figures 2–5 were made with respect to tem-

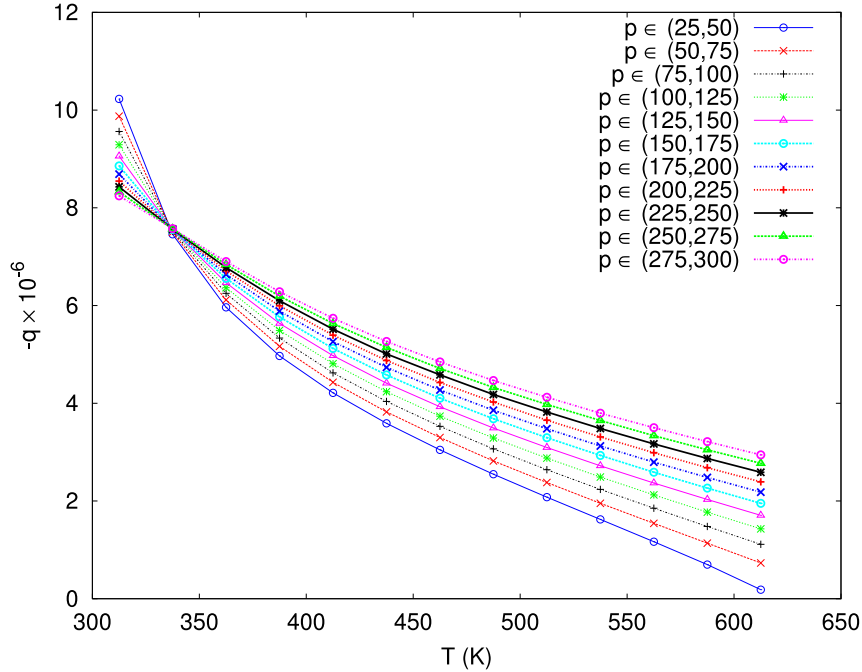


Figure 3: Plots of  $-q \times 10^{-6}$  (J/kg) vs. temperature for different pressure ranges, all pressure ranges are in MPa.

perature, we found the error plots were easier to understand (and explain) when plotted with respect to pressure. The errors in the temperature fits are less than about 2% over the entire range of pressures and temperatures investigated. The temperature error bounds improve with increasing temperature, except for the highest temperatures at the lowest pressures, where the error begins increasing rapidly. The latter situation (high temperatures and lower pressures) corresponds to a region of the phase space diagram which is closer to the liquid-vapor transition line, and therefore to an area in which the stiffened gas equation of state is not particularly well-suited.

The trend of higher error being present in the fits at lower pressures is also evident in Fig. 7, although in this case the maximum relative error is slightly above 5%. The error decreases rapidly at higher pressures, however, which is in contrast to the nearly-constant error levels seen in the temperature fits. We conjecture that this behavior is primarily due to the “decoupled” strategy employed in computing the fits (described in §2). Although our fits only extend to 300 MPa, we fully expect the trend of low relative errors in

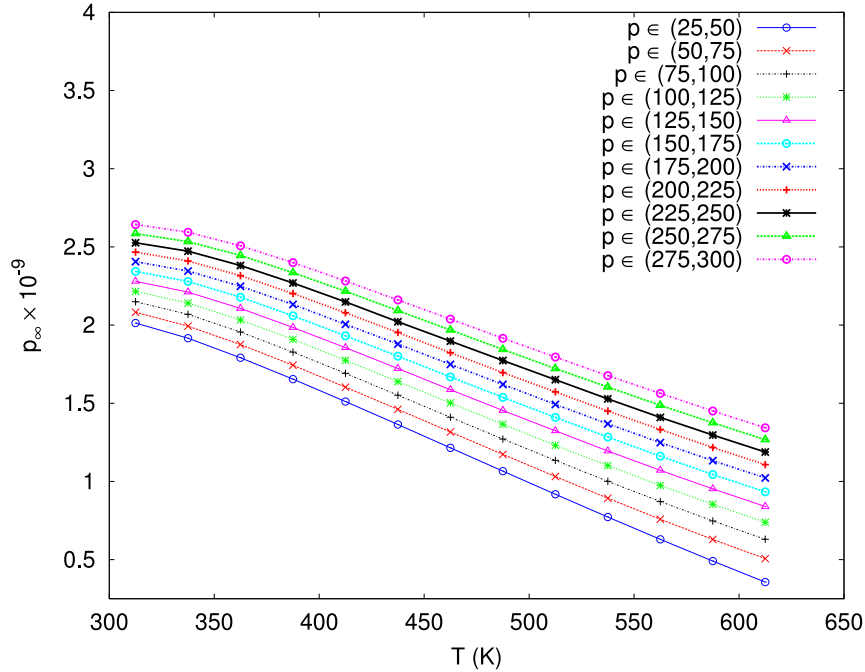


Figure 4: Plots of  $p_\infty \times 10^{-9}$  (Pa) vs. temperature for different pressure ranges, all pressure ranges are in MPa.

the pressure fits to continue out to much higher pressures.

## 4 Conclusion

A method for computing optimal linear least-squares curve fits for the stiffened gas equation of state over a wide range of pressures and temperatures was presented, along with relative error bounds for both. For high pressures and temperatures, reasonable accuracy in both the pressure and temperature models is obtained; the curve fits are unfortunately much less accurate near the liquid-vapor transition line. The tabulated parameter values presented here are practical for use in codes attempting to simulate water as a compressible liquid.

We remark that the data in this paper should *not* be used to conclude that a more complex equation of state, for example with pressure- and temperature-dependent parameters, should be utilized in place of the much

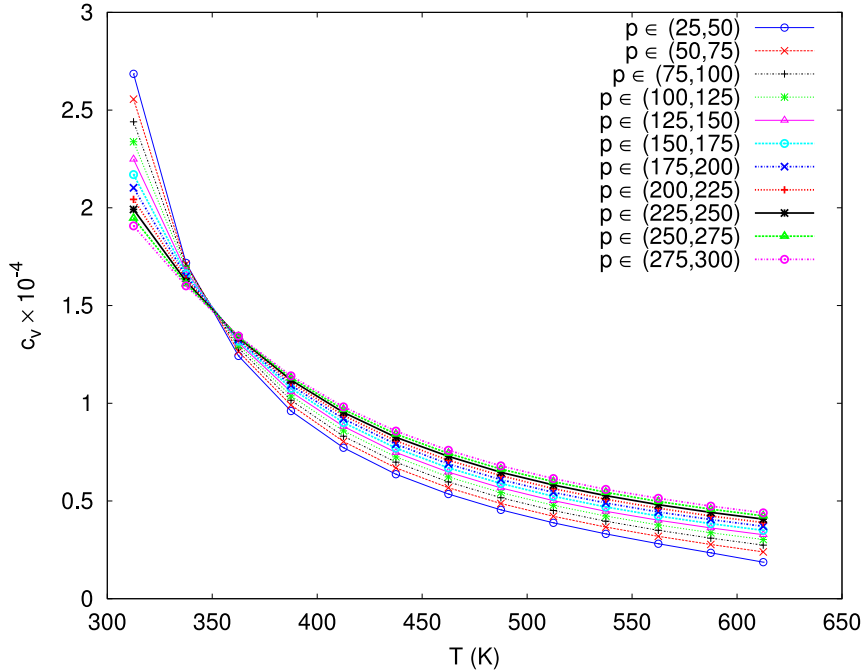
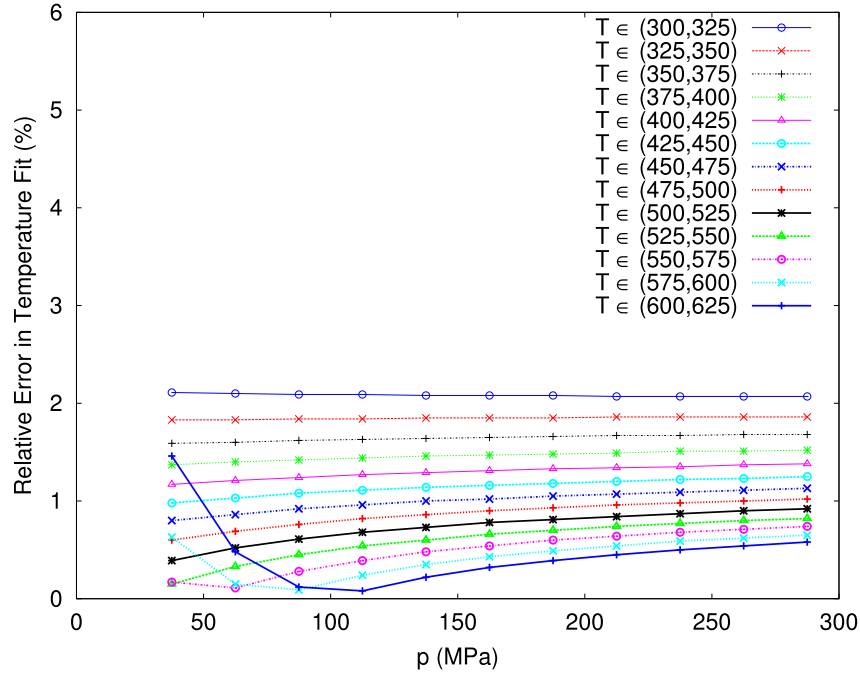


Figure 5: Plots of  $c_v \times 10^{-4}$  (J/kg-K) vs. temperature for different pressure ranges, all pressure ranges are in MPa.

simpler stiffened gas equation of state. Rather, we recommend that this data be used in the following way: given *a priori* knowledge of a particular problem, for example operational pressure and temperature ranges, appropriate constant values of  $\gamma$ ,  $q$ ,  $p_\infty$ , and  $c_v$  should be selected from Tables 1–4 and used in the computation. Of course, if the operational pressure or temperature for a given problem exceeds the 25 MPa or 25 K ranges presented in the tables, some sort of averaging process (based on the tabulated data) should be employed to select the constant values.

The importance of having accurate equation of state values in fluid dynamics simulations is difficult to quantify, and of course problem-dependent. Parameter sensitivity analysis of nonlinear partial differential equations is itself an important area of ongoing research [11], and is presently the best way of determining, for a given problem, how errors in parameter values translate to errors in problem quantities of interest. The parametric sensitivity analysis of pressure equation of state values for the Euler equations is also complicated by the fact that e.g. the flux Jacobians also involve derivatives



(a)  $\varepsilon_T$

Figure 6: Plots of the relative error  $\varepsilon_T$  vs. pressure for different temperature ranges, all temperature ranges are in K.

of the pressure with respect to the conserved variables. While such an analysis is clearly beyond the scope of the present paper, we feel it represents an interesting avenue of future work.

## Acknowledgments

The submitted manuscript has been authored by a contractor of the U.S. Government under Contract DE-AC07-05ID14517. Accordingly, the U.S. Government retains a non-exclusive, royalty-free license to publish or reproduce the published form of this contribution, or allow others to do so, for U.S. Government purposes.

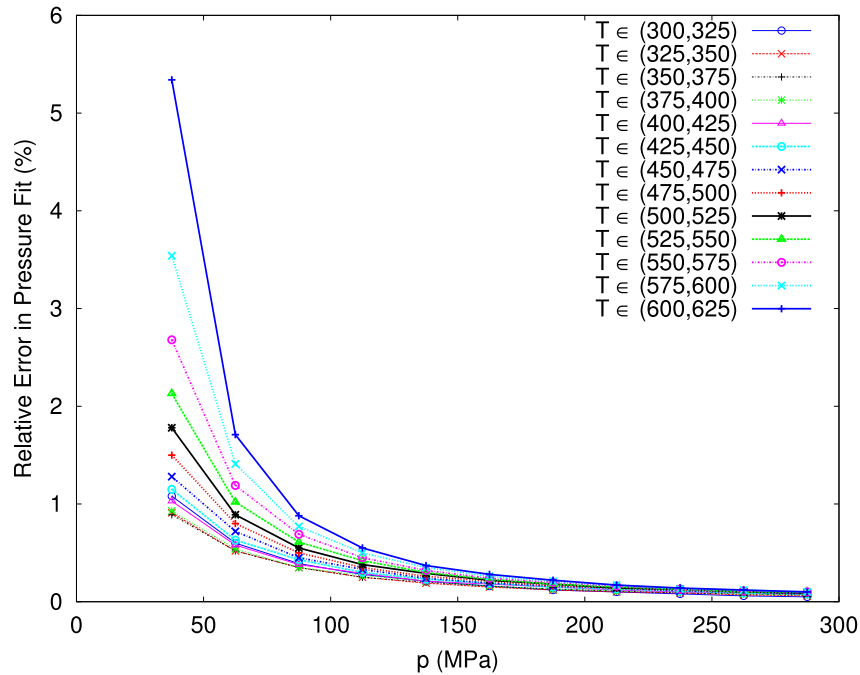


Figure 7: Plots of the relative error  $\varepsilon_p$  vs. pressure for different temperature ranges, all temperature ranges are in K.

## References

- [1] R. A. Berry, R. Saurel, and O. L. Métayer, “The discrete equation method (DEM) for fully compressible, two-phase flows in ducts of spatially varying cross-section,” *Nuclear Engineering and Design*, vol. 240, pp. 3797–3818, Nov. 2010. <http://dx.doi.org/10.1016/j.nucengdes.2010.08.003>.
- [2] R. Menikoff and B. J. Plohr, “The Riemann problem for fluid flow of real materials,” *Reviews of Modern Physics*, vol. 61, no. 1, pp. 75–130, 1989. <http://dx.doi.org/10.1103/RevModPhys.61.75>.
- [3] O. L. Métayer, J. Massoni, and R. Saurel, “Elaborating equations of state of a liquid and its vapor for two-phase flow models,” *Int. J. Thermal Sciences (in French)*, vol. 43, pp. 265–276, Mar. 2004. <http://dx.doi.org/10.1016/j.ijthermalsci.2003.09.002>.

- [4] J. H. Dymond and R. Malhotra, “The Tait equation: 100 years on,” *International Journal of Thermophysics*, vol. 9, no. 6, pp. 941–951, 1988. <http://dx.doi.org/10.1007/BF01133262>.
- [5] R. Saurel, J. P. Cocchi, and P. B. Butler, “Numerical study of cavitation in the wake of a hypervelocity underwater projectile,” *J. of Propulsion and Power*, vol. 15, pp. 512–522, July 1999.
- [6] Wikipedia, “Phase diagram,” 2012. [http://en.wikipedia.org/wiki/Phase\\_diagram](http://en.wikipedia.org/wiki/Phase_diagram), [Online; accessed 01-Nov-2012].
- [7] R. E. Steuer, *Multiple criteria optimization: theory, computations, and application*. New York: John Wiley & Sons, Inc., 1986.
- [8] D. Fudenberg and J. Tirole, *Game Theory. Chapter 1, Section 2.4*. Cambridge, Mass: MIT Press, 1983.
- [9] A. Saul and W. Wagner, “A fundamental equation for water covering the range from the melting line to 1273 K at pressures up to 25000 MPa,” *Journal of Physical and Chemical Reference Data*, vol. 18, no. 4, pp. 1537–1564, 1989. <http://www.nist.gov/data/PDFfiles/jpcrd370.pdf>.
- [10] W. Wagner and A. Pruss, “The IAPWS formulation 1995 for the thermodynamic properties of ordinary water substance for general and scientific use,” *Journal of Physical and Chemical Reference Data*, vol. 31, no. 2, pp. 387–535, 2002. [http://www.teos-10.org/pubs/Wagner\\_and\\_Pruss\\_2002.pdf](http://www.teos-10.org/pubs/Wagner_and_Pruss_2002.pdf).
- [11] M. Anderson, W. Bangerth, and G. F. Carey, “Analysis of parameter sensitivity and experimental design for a class of nonlinear partial differential equations,” *Int. J. Numer. Meth. Fluids*, vol. 48, pp. 583–605, 2005. <http://dx.doi.org/10.1002/flid.938>.

Table 1: Values of  $\gamma$  for various pressure (rows) and temperature (columns) ranges.

		Temperature Ranges (K)												
		300-325	325-350	350-375	375-400	400-425	425-450	450-475	475-500	500-525	525-550	550-575	575-600	600-625
Pressure Ranges (MPa)	25-50	1.2424	1.3381	1.4135	1.4712	1.5140	1.5442	1.5618	1.5698	1.5684	1.5590	1.5429	1.5207	1.5014
	50-75	1.2637	1.3538	1.4263	1.4822	1.5247	1.5556	1.5741	1.5849	1.5860	1.5804	1.5687	1.5517	1.5305
	75-100	1.2855	1.3696	1.4384	1.4935	1.5361	1.5654	1.5848	1.5966	1.6008	1.5982	1.5898	1.5768	1.5604
	100-125	1.3074	1.3856	1.4512	1.5049	1.5450	1.5751	1.5969	1.6088	1.6135	1.6137	1.6069	1.5969	1.5830
	125-150	1.3292	1.4018	1.4638	1.5152	1.5551	1.5862	1.6061	1.6197	1.6262	1.6263	1.6221	1.6135	1.6026
	150-175	1.3507	1.4178	1.4767	1.5259	1.5653	1.5951	1.6162	1.6292	1.6366	1.6386	1.6355	1.6286	1.6192
	175-200	1.3718	1.4337	1.4894	1.5368	1.5748	1.6048	1.6261	1.6405	1.6472	1.6497	1.6474	1.6415	1.6331
	200-225	1.3924	1.4494	1.5020	1.5475	1.5846	1.6145	1.6347	1.6475	1.6571	1.6598	1.6588	1.6539	1.6456
	225-250	1.4124	1.4647	1.5143	1.5580	1.5942	1.6223	1.6418	1.6577	1.6658	1.6687	1.6674	1.6634	1.6567
	250-275	1.4318	1.4798	1.5267	1.5686	1.6035	1.6311	1.6517	1.6658	1.6729	1.6774	1.6773	1.6740	1.6676
	275-300	1.4507	1.4947	1.5386	1.5787	1.6127	1.6397	1.6596	1.6736	1.6821	1.6868	1.6868	1.6835	1.6777

91

Table 2: Table of  $-q \times 10^{-6}$  values for various pressure (rows) and temperature (columns) ranges.

		Temperature Ranges (K)												
		300-325	325-350	350-375	375-400	400-425	425-450	450-475	475-500	500-525	525-550	550-575	575-600	600-625
Pressure Ranges (MPa)	25-50	10.229	7.4583	5.9632	4.9684	4.2132	3.5888	3.0462	2.5478	2.0786	1.6228	1.1668	0.6981	0.1848
	50-75	9.8755	7.4981	6.1147	5.1651	4.4294	3.8227	3.2988	2.8197	2.3782	1.9534	1.5427	1.1368	0.7313
	75-100	9.5622	7.5243	6.2503	5.3350	4.6227	4.0381	3.5282	3.0660	2.6412	2.2377	1.8526	1.4788	1.1140
	100-125	9.2909	7.5404	6.3650	5.4912	4.8095	4.2369	3.7354	3.2894	2.8774	2.4897	2.1245	1.7713	1.4302
	125-150	9.0570	7.5490	6.4663	5.6351	4.9747	4.4108	3.9286	3.4929	3.0951	2.7200	2.3684	2.0318	1.7061
	150-175	8.8574	7.5549	6.5561	5.7668	5.1212	4.5792	4.1039	3.6825	3.2950	2.9321	2.5882	2.2640	1.9522
	175-200	8.6898	7.5581	6.6373	5.8862	5.2607	4.7347	4.2708	3.8573	3.4790	3.1262	2.7948	2.4823	2.1806
	200-225	8.5469	7.5620	6.7110	5.9958	5.3943	4.8756	4.4251	4.0254	3.6531	3.3108	2.9879	2.6815	2.3917
	225-250	8.4281	7.5648	6.7784	6.0979	5.5164	5.0104	4.5814	4.1800	3.8214	3.4837	3.1681	2.8705	2.5872
	250-275	8.3278	7.5687	6.8403	6.1928	5.6319	5.1434	4.7126	4.3229	3.9754	3.6472	3.3373	3.0477	2.7709
	275-300	8.2448	7.5748	6.8996	6.2827	5.7397	5.2651	4.8461	4.4662	4.1225	3.7963	3.5001	3.2141	2.9442



Table 3: Table of  $p_\infty \times 10^{-9}$  values for various pressure (rows) and temperature (columns) ranges.

		Temperature Ranges (K)												
		300-325	325-350	350-375	375-400	400-425	425-450	450-475	475-500	500-525	525-550	550-575	575-600	600-625
Pressure Ranges (MPa)	25-50	2.0132	1.9161	1.7911	1.6543	1.5109	1.3641	1.2150	1.0659	0.9181	0.7725	0.6299	0.4908	0.3565
	50-75	2.0822	1.9936	1.8757	1.7433	1.6030	1.4608	1.3162	1.1732	1.0316	0.8925	0.7582	0.6290	0.5064
	75-100	2.1495	2.0685	1.9556	1.8269	1.6915	1.5514	1.4105	1.2713	1.1350	1.0008	0.8713	0.7472	0.6301
	100-125	2.2155	2.1409	2.0329	1.9082	1.7750	1.6386	1.5023	1.3657	1.2309	1.1011	0.9746	0.8538	0.7389
	125-150	2.2800	2.2110	2.1066	1.9845	1.8555	1.7221	1.5867	1.4540	1.3237	1.1944	1.0713	0.9524	0.8398
	150-175	2.3434	2.2791	2.1785	2.0595	1.9314	1.8011	1.6685	1.5375	1.4096	1.2841	1.1614	1.0446	0.9335
	175-200	2.4056	2.3453	2.2482	2.1321	2.0050	1.8787	1.7486	1.6207	1.4924	1.3685	1.2482	1.1331	1.0226
	200-225	2.4667	2.4101	2.3158	2.2017	2.0785	1.9526	1.8232	1.6960	1.5726	1.4504	1.3321	1.2173	1.1076
	225-250	2.5262	2.4725	2.3810	2.2692	2.1485	2.0212	1.8973	1.7734	1.6506	1.5281	1.4096	1.2967	1.1884
	250-275	2.5851	2.5338	2.4450	2.3355	2.2164	2.0929	1.9686	1.8440	1.7219	1.6037	1.4869	1.3755	1.2671
	275-300	2.6430	2.5939	2.5071	2.3995	2.2822	2.1608	2.0383	1.9155	1.7957	1.6767	1.5631	1.4506	1.3432

11

Table 4: Table of  $c_v \times 10^{-4}$  values for various pressure (rows) and temperature (columns) ranges.

		Temperature Ranges (K)												
		300-325	325-350	350-375	375-400	400-425	425-450	450-475	475-500	500-525	525-550	550-575	575-600	600-625
Pressure Ranges (MPa)	25-50	2.6854	1.7178	1.2425	0.9604	0.7724	0.6372	0.5356	0.4546	0.3882	0.3316	0.2814	0.2349	0.1871
	50-75	2.5560	1.7112	1.2644	0.9907	0.8041	0.6692	0.5681	0.4870	0.4219	0.3667	0.3193	0.2774	0.2395
	75-100	2.4401	1.7015	1.2834	1.0157	0.8314	0.6988	0.5975	0.5168	0.4514	0.3967	0.3502	0.3098	0.2742
	100-125	2.3380	1.6896	1.2976	1.0381	0.8587	0.7258	0.6231	0.5431	0.4779	0.4231	0.3774	0.3375	0.3028
	125-150	2.2484	1.6762	1.3092	1.0587	0.8817	0.7482	0.6477	0.5671	0.5018	0.4474	0.4016	0.3623	0.3276
	150-175	2.1701	1.6628	1.3182	1.0767	0.9014	0.7706	0.6693	0.5895	0.5242	0.4696	0.4234	0.3841	0.3498
	175-200	2.1025	1.6491	1.3256	1.0922	0.9202	0.7906	0.6896	0.6093	0.5443	0.4898	0.4439	0.4048	0.3705
	200-225	2.0431	1.6361	1.3316	1.1061	0.9377	0.8082	0.7086	0.6296	0.5633	0.5091	0.4629	0.4234	0.3896
	225-250	1.9919	1.6235	1.3365	1.1187	0.9534	0.8259	0.7283	0.6469	0.5819	0.5273	0.4812	0.4416	0.4073
	250-275	1.9469	1.6116	1.3403	1.1298	0.9681	0.8425	0.7434	0.6633	0.5992	0.5443	0.4978	0.4582	0.4238
	275-300	1.9077	1.6007	1.3440	1.1403	0.9815	0.8575	0.7595	0.6798	0.6149	0.5594	0.5137	0.4738	0.4394